Quantum thermometry in diffraction-limited systems

Dong Xie [1,2,*] Chunling Xu,[1] and An Min Wang [3]

[1]*College of Science, Guilin University of Aerospace Technology, Guilin, Guangxi 541004, People's Republic of China*
[2]*State Key Laboratory for Mesoscopic Physics, School of Physics,*
Frontiers Science Center for Nano-Optoelectronics,
and Collaborative Innovation Center of Quantum Matter,
Peking University, Beijing 100871, People's Republic of China
[3]*Department of Modern Physics, University of Science and Technology of China,*
Hefei, Anhui 230026, People's Republic of China

We investigate the ultimate quantum limit of resolving the temperatures of two thermal sources affected by diffraction. More quantum Fisher information can be obtained with *a priori* information than without *a priori* information. We carefully consider two strategies: simultaneous estimation and individual estimation. We prove that the simultaneous estimation of two temperatures satisfies the saturation condition of the quantum Cramér-Rao bound and performs better than the individual estimation in the case of a small degree of diffraction given the same resources. However, in the case of a high degree of diffraction, the individual estimation performs better. In particular, at the maximum diffraction, the simultaneous estimation cannot get any information, which is supported by a practical measurement, while the individual estimation can still get the information. In addition, we find that for the individual estimation, a practical and feasible estimation strategy using the full Hermite-Gauss basis can saturate the quantum Cramér-Rao bound without being affected by the attenuation factor at the maximum diffraction.

I. INTRODUCTION

In classical optics, optical imaging resolution is limited by the diffraction. For over a century, Rayleigh's criterion was used as a limit of the resolution of two incoherent point sources [1,2]. In the last decade, the limit has been beaten by a variety of super-resolution techniques, such as fluorescence microscopy [3–5].

Tsang *et al.* [6] first investigated the imaging resolution limit with the tool of quantum metrology. They obtained the lower bound of the separation between two incoherent point sources and showed that the spatial-mode demultiplexing can approach the optimal measurement, which is superior to direct measurement. This seminal work opened up a wide range of interest in exploring quantum imaging using quantum Fisher information (QFI). The studies that followed mainly extended the super-resolution technique to deal with two-dimensional [7] and three-dimensional imaging [8–11], many sources [12–16], the effects of noise [17,18], and optimal measurement for practical super-resolution imaging [19].

Up to now, very little work has been done to investigate the effect of diffraction on quantum thermometry, which mainly involves improving precision standards for temperature sensing in the quantum regime [20]. Improving temperature measurement precision is important in quantum thermodynamics and modern quantum technology [21–23]. The commercially available pyrometer is one of the most common noncontact thermometers and measures the thermal infrared radiation naturally emitted by all heated samples [24,25]. As with quantum imaging, it is necessary to study the effect of diffraction on temperature measurement precision to obtain the optimal temperature measurement.

In this paper, we fill in the gaps above. We investigate the ultimate quantum limit of resolving the temperatures of two thermal sources affected by diffraction. When one knows *a priori* that the two temperatures are always the same, the maximum diffraction reduces the QFI of the high temperature by half, and the diffraction has little effect on the measurement of the low temperature. We find that the *a priori* information can help us to obtain twice as much QFI as can be obtained without the *a priori* information (the two temperatures are independent). More importantly, we find that simultaneous estimation is superior to individual estimation in the case of a small degree of diffraction. In the case of a high degree of diffraction, individual estimation can perform better. In addition, we utilize a practical and feasible estimation strategy based on the optimized error transfer formula to obtain the individual temperature estimation uncertainty, which can saturate the quantum Cramér-Rao bound (QCRB) at the maximum diffraction. Finally, we show that the diffraction will reduce the precision of the simultaneous estimation with a practical measurement operator, which cannot obtain any information at the maximum diffraction.

This paper is organized as follows. In Sec. II, we introduce the imaging model and the density matrix in which
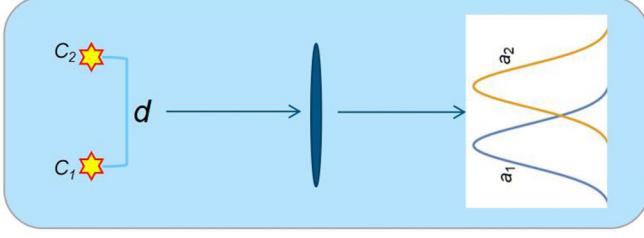
---

*xiedong@mail.ustc.edu.cn

FIG. 1. Schematic diagram of the diffraction-limited imaging of thermal states from two pointlike sources. The two sources' modes $c_{1(2)}$ describe the light from the two thermal sources with distance d and are populated with photon numbers $N(1 \pm \gamma)$. $a_{1(2)}$ are the nonorthogonal imaging modes due to the diffraction.

temperature information is encoded. In Sec. III, we obtain the QFI when the two thermal sources have the same temperature. In Sec. IV, simultaneous estimation and individual estimation are used to obtain the QFI, and we compare the merits of the two strategies. In Sec. V, we investigate a practical and feasible estimation of a single parameter. In Sec. VI, we calculate the Fisher information (FI) obtained by the direct imaging. The simultaneous estimation with a practical measurement operator is studied in Sec. VII. We present a brief conclusion and feasibility analysis in Sec. VIII.

II. THE IMAGING MODEL

We consider the model of a linear optical imaging system in the far field, as shown in Fig. 1. Two thermal pointlike sources are monochromatic with frequency ω and located in the object plane, orthogonal to the optical axis, at positions $-d/2$ and $d/2$. We define T_1 and T_2 as temperatures of the two sources associated with the field operators c_1 and c_2, respectively. We assume that the two sources emit a total mean photon number equal to $2N$, where $N = \frac{1}{2}[1/(\chi_1 - 1) + 1/(\chi_2 - 1)]$ with $\chi_i = e^{\omega/T_i}$ (the reduced Planck constant $\hbar = 1$ and Boltzmann constant $\kappa_B = 1$ throughout this paper). The sources can be described by the density matrix $\rho_0 = \rho_{c_1}[(1 - \gamma)N] \otimes \rho_{c_2}[(1 + \gamma)N]$, where $\gamma = (\chi_1 - \chi_2)/(\chi_1 + \chi_2)$ takes into account the possibly different temperatures of the two sources. In the Glauber-Sudarshan P representation, the density matrix can also be described by

$$\rho_0 = \int d^2\alpha_1 d^2\alpha_2 P_{c_1,c_2}(\alpha_1, \alpha_2)|\alpha_1, \alpha_2\rangle\langle\alpha_1, \alpha_2|, \quad (1)$$

where $|\alpha_1\rangle$ and $|\alpha_2\rangle$ are coherent states of the field operators c_1 and c_2, respectively, and the Glauber-Sudarshan P function is $P_{c_1,c_2}(\alpha_1, \alpha_2) = P_{c_1}(\alpha_1)P_{c_2}(\alpha_2)$, with

$$P_{c_1,c_2}(\alpha_1, \alpha_2) = \frac{1}{\pi^2 N^2(1 - \gamma^2)} e^{[-|\alpha_1|^2/(1-\gamma)-|\alpha_2|^2/(1+\gamma)]}. \quad (2)$$

The point-spread function $\psi(x)$ determines the field operators on the image plane, which read

$$a_1^\dagger = \int dx\psi(x + d/2)a_x^\dagger, \quad a_2^\dagger = \int dx\psi(x - d/2)a_x^\dagger, \quad (3)$$

where $a_x^\dagger$ is the canonical creation operator for a field localized at position x on the image plane, and the point-spread function $\psi(x)$ is assumed to be real up to a global phase.

A diffraction-limited optical system transforms the source operators as [26]

$$c_1 \longrightarrow \sqrt{\eta}a_1 + \sqrt{1 - \eta}v_1, \quad (4)$$

$$c_2 \longrightarrow \sqrt{\eta}a_2 + \sqrt{1 - \eta}v_2, \quad (5)$$

where η is an attenuation factor and v_1 and v_2 are auxiliary environmental modes in the vacuum state.

The operators $c_1^\dagger$ and c_2 do not commute due to the nonzero overlap between the two point-spread functions $\psi(x + d/2)$ and $\psi(x - d/2)$. To obviate this problem, the orthonormal image modes are introduced:

$$\psi_\pm(x) = \frac{\psi(x + d/2) \pm \psi(x - d/2)}{\sqrt{2(1 \pm s)}}, \quad (6)$$

where s is the overlap between the source images

$$s = \int d^2x\psi^*(x + d/2)\psi(x - d/2). \quad (7)$$

s quantifies the diffraction introduced by the imaging optical system. $s = 1$ represents the maximum diffraction. $s = 0$ means that there is no diffraction. By taking the sum and difference of the relations in Eqs. (4) and (5), one can obtain

$$c_\pm := \frac{c_1 \pm c_2}{\sqrt{2}} \to \sqrt{\eta_\pm}a_\pm + \sqrt{1 - \eta_\pm}v_\pm, \quad (8)$$

where $a_\pm = (a_1 \pm a_2)/\sqrt{2(1 \pm s)}$ are orthogonal symmetric and antisymmetric mode operators associated with the modes $\psi_\pm(x)$ and the effective attenuation factors are $\eta_\pm = \eta(1 \pm s)$ and $v_\pm$ associated with auxiliary modes in the vacuum state. Inverting Eq. (8), we can write

$$a_\pm := \sqrt{\eta_\pm}c_\pm + \sqrt{1 - \eta_\pm}v_\pm. \quad (9)$$

The density matrix on the image plane can be obtained by using Eq. (9) to propagate the quantum state of source in Eq. (1) [27], as shown in the Appendix,

$$\rho = \int d^2\alpha_+ d^2\alpha_- P_{a_+,a_-}(\alpha_+, \alpha_-)|\alpha_+, \alpha_-\rangle\langle\alpha_+, \alpha_-|, \quad (10)$$

where the corresponding P function is

$$P_{a_+,a_-}(\alpha_+, \alpha_-) = \frac{1}{\pi^2 \det V} e^{-\mathbf{A}^\dagger V^{-1}\mathbf{A}}, \quad (11)$$

with the definition $\mathbf{A} = (\alpha_+, \alpha_-)^T$ and

$$V = \begin{pmatrix} N_+ & \gamma\sqrt{N_+N_-} \\ \gamma\sqrt{N_+N_-} & N_- \end{pmatrix},$$

in which, $N_\pm = N\eta(1 \pm s)$.

III. TWO THERMAL SOURCES WITH THE SAME TEMPERATURE

We first consider that temperatures of the two sources are always the same, i.e., $T_1 = T_2 = T$. According to Eq. (11), the density matrix on the image plane is a product state, which can be described in the number-diagonal states of the form

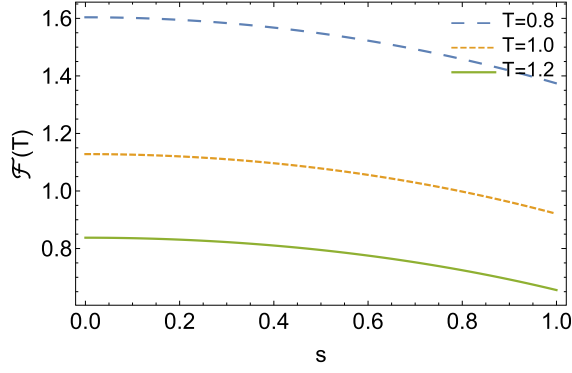$$\rho = \rho_+ \otimes \rho_-, \quad (12)$$

FIG. 2. The QFI $\mathcal{F}(T)$, computed from Eq. (16), vs the degree of diffraction s. The dimensionless parameters are given by $\omega = 1$ and $\eta = 0.5$.

with the density matrices associated with the field operators $a_\pm$

$$\rho_\pm = \sum_{n=0}^{\infty} p_\pm(n)|n\rangle_\pm \langle n|, \tag{13}$$

where

$$p_\pm(n) = \frac{(M_\pm)^n}{(M_\pm + 1)^{n+1}}, \tag{14}$$

$M_\pm = \frac{\eta(1\pm s)}{e^{\omega/T}-1}$, and $|n\rangle_\pm = \frac{1}{\sqrt{n!}}(a_\pm^\dagger)^n|0\rangle$ denote Fock states with n photons on the image plane. Because it is a diagonal state, the QFI of the temperature T can be directly calculated:

$$\mathcal{F}(T) = \sum_{n=0}^{\infty} \frac{[\partial_T p_+(n)]^2}{p_+(n)} + \frac{[\partial_T p_-(n)]^2}{p_-(n)} \tag{15}$$

$$= \frac{2\chi^2\omega^2\eta(\chi - 1 + \eta - s^2\eta)}{(\chi - 1)^2 T^4(-1 + \chi + \eta - s\eta)(-1 + \chi + \eta + s\eta)}, \tag{16}$$

where the shorthand $\partial_T = \frac{\partial}{\partial T}$ and $\chi = e^{\omega/T}$.

At low temperature $\omega/T \gg 1$, we can achieve

$$\mathcal{F}(T) = \frac{2\omega^2\eta}{T^4 e^{\omega/T}}. \tag{17}$$

It is independent of the degree of diffraction s, which can show that the diffraction has little effect on the measurement of low temperature.

At high temperature, $\omega/T \ll 1$, we can obtain

$$\mathcal{F}(T) \approx \frac{2\eta[\omega/T + \eta(1 - s^2)]}{T^2[\omega/T + \eta(1 - s)][\omega/T + \eta(1 + s)]}. \tag{18}$$

In this case, we find that $\mathcal{F}(T)|_{s=1}/\mathcal{F}(T)|_{s=0} = 1/2$. This means that the maximum diffraction reduces the QFI by half.

In the general case, we can see that the diffraction will reduce the QFI of the temperature as shown in Fig. 2. At the maximum diffraction, we still obtain a finite QFI. This demonstrates that the diffraction has no great influence on temperature measurement in the case of two thermal sources with the same temperature.

IV. ESTIMATING TWO DIFFERENT TEMPERATURES

In this section, we want to estimate the temperatures T_1 and T_2 of the two thermal sources. In this case, the two temperatures are independent. The estimation precision of (T_1, T_2), governed by its covariance matrix $\mathrm{Cov}(T_1, T_2)$, is lower bounded via the QCRB [28]

$$\mathrm{Cov}(T_1, T_2) \geqslant (\nu\mathcal{H})^{-1}, \tag{19}$$

where $\mathcal{H}$ is the QFI matrix and ν denotes the classical contribution from repeating the experiment. There are two measurement strategies: One is the simultaneous estimation of the two temperatures, and the other is the individual estimation of the two temperatures. A lot of works [29–38] have clearly shown that simultaneous estimation can be more precise than individual estimation given the same resource. We are going to look at whether this is true in the diffraction case.

For the simultaneous estimation, the total estimation uncertainty of the two temperatures is given by

$$(\delta^2 T_1 + \delta^2 T_2)|_{\mathrm{sim}} = \mathrm{tr}[\mathrm{Cov}(T_1, T_2)] \geqslant \mathrm{tr}(\nu\mathcal{H})^{-1}$$

$$= \frac{1}{\nu} \frac{\mathcal{H}^{11} + \mathcal{H}^{22}}{\mathcal{H}^{11}\mathcal{H}^{22} - |\mathcal{H}^{12}|^2}, \tag{20}$$

where $\mathcal{H}^{ij}$ $(i, j = 1, 2)$ represent the elements of the QFI matrix $\mathcal{H}$.

For the individual estimation, the estimation uncertainties of the two temperatures are given by

$$\delta^2 T_1|_{\mathrm{ind}} \geqslant \frac{1}{\nu/2} \frac{1}{\mathcal{H}^{11}}, \tag{21}$$

$$\delta^2 T_2|_{\mathrm{ind}} \geqslant \frac{1}{\nu/2} \frac{1}{\mathcal{H}^{22}}, \tag{22}$$

where we consider that T_1 and T_2 are individually measured $\nu/2$ times so that the total number of measurements is consistent with the case of simultaneous estimation. In the case of individual estimation, the lower bound in Eqs. (21) and (22) can be saturated with the large number of repeated measurements ($\nu \gg 1$).

In the case of simultaneous estimation, the lower bound in Eq. (20) is saturated by satisfying the weak commutation relation when collective measurements on multiple copies of samples are permitted [39–42], which is described as [43]

$$\mathrm{tr}(\rho[\mathcal{L}_1, \mathcal{L}_2]) = 0, \tag{23}$$

where $\mathcal{L}_i$ $(i = 1, 2)$ are the symmetric logarithmic derivatives, which are defined as operator solutions of equations $\partial_i\rho = \frac{1}{2}(\mathcal{L}_i\rho + \rho\mathcal{L}_i)$, where $\partial_i = \partial_{T_i}$ denotes the partial derivative with respect to the ith element of the vector of estimated parameters (T_1, T_2).

The quantum state ρ is a Gaussian state. For the Gaussian state, the QFI matrix $\mathcal{H}$ and symmetric logarithmic derivatives can be described as [44]

$$\mathcal{H}^{ij} = \frac{1}{2}\mathrm{vec}[\partial_i\sigma]^\dagger \mathcal{R}^{-1}\mathrm{vec}[\partial_j\sigma] + 2\partial_i\mathbf{d}^\dagger\sigma^{-1}\partial_j\mathbf{d}, \tag{24}$$

$$\mathcal{L}_i = \Delta\mathbf{A}^\dagger\mathcal{R}^{-1}\mathrm{vec}[\partial_i\sigma]\Delta\mathbf{A} - \frac{1}{2}\mathrm{tr}(\sigma\mathcal{R}^{-1}\mathrm{vec}[\partial_i\sigma])$$

$$+ 2\Delta\mathbf{A}^\dagger\sigma^{-1}\partial_i\mathbf{d}, \tag{25}$$

where the elements of the displacement vector $\mathbf{d}$ and the covariant matrix σ are defined as $d_i = \text{tr}[\rho A_i]$ and $\sigma_{ij} = \text{tr}\{\rho \Delta A_i, \Delta A_j\}$, $\mathbf{A} = (a_+, a_-, a_+^\dagger, a_-^\dagger)^T$, $\Delta A_i = A_i - d_i$, $\mathcal{R}^{-1} = \bar{\sigma} \otimes \sigma - \mathbf{K} \otimes \mathbf{K}$, and $\mathbf{K} = \text{diag}(1, 1, -1, -1)$. The overbar, as in $\bar{\sigma}$, denotes the complex conjugate, and $\{\cdot, \cdot\}$ denotes the anticommutator. $\text{vec}[\cdot]$ denotes vectorization of a matrix, which is defined as a column vector constructed from columns of a matrix. By calculation, the variance matrix can be achieved:

$$\sigma = \begin{pmatrix} 2N_+ + 1 & -2\gamma\sqrt{N_+ N_-} & 0 & 0 \\ -2\gamma\sqrt{N_+ N_-} & 2N_- + 1 & 0 & 0 \\ 0 & 0 & 2N_+ + 1 & -2\gamma\sqrt{N_+ N_-} \\ 0 & 0 & -2\gamma\sqrt{N_+ N_-} & 2N_- + 1 \end{pmatrix}.$$

A. Increasing QFI with the *a priori* information

When we have the *a priori* information, we know *a priori* that the two temperatures of the two sources are always equal, i.e., $T_1 = T_2$. With the *a priori* information, the saturated uncertainty of T_1 is given by

$$\delta^2 T_1|_{\text{pri}} = \frac{1}{\nu/2}\frac{1}{\mathcal{F}(T_1)}, \tag{26}$$

where the QFI $\mathcal{F}(T_1)$ is described in Eq. (16).

Without the *a priori* information, when $T_2 \to T_1$, we can obtain the analytical results of the QFI matrix based on Eq. (24):

$$\mathcal{H}^{11}(T_2 \to T_1)$$
$$= \mathcal{H}^{22}(T_2 \to T_1)$$
$$= \frac{\chi_1^2 \omega^2 \eta}{T_1^4(\chi_1 - 1)^2[(1 - \chi_1 - \eta)^2 - s^2\eta^2](-1 + \chi_1 + \eta - s^2\eta)}$$
$$\times \big[(1 + \chi_1^2)(s^2 - 2) - 2(s^2 - 1)^2\eta^2 - 4(s^2 - 1)\eta$$
$$+ \chi_1(4 - 4\eta + s^2(4\eta - 2))\big]. \tag{27}$$

In this case, the uncertainty of the temperature T_1 is

$$\delta^2 T_1|_{\text{ind}} = \frac{1}{\nu/2}\frac{1}{\mathcal{H}^{11}(T_2 \to T_1)}. \tag{28}$$

When there is no diffraction ($s = 0$), $\mathcal{F}(T_1) = \mathcal{H}^{11}(T_2 \to T_1) + \mathcal{H}^{22}(T_2 \to T_1) = 2\mathcal{H}^{11}(T_2 \to T_1)$. However, when there is diffraction ($s \neq 0$), $\mathcal{F}(T_1) > 2\mathcal{H}^{11}(T_2 \to T_1)$, as shown in Fig. 3. In particular, when $s = 1$, $\mathcal{F}(T_1) = 2(\mathcal{H}^{11} + \mathcal{H}^{22}) = 4\mathcal{H}^{11}$. This shows that more QFI can be obtained with the *a priori* information of $T_1 = T_2$ than
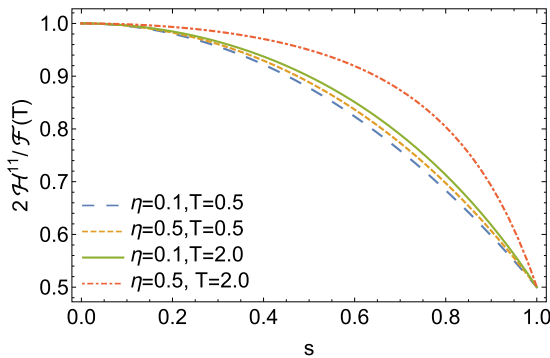
without the *a priori* information when subjected to diffraction. At the maximum diffraction ($s = 1$), the *a priori* information can help us to obtain twice as much QFI as can be obtained without the *a priori* information.

B. Simultaneous estimation versus individual estimation

For simultaneous estimation, we show that the lower bound in Eq. (20) can be saturated by analytically deriving

$$\text{tr}(\rho[\mathcal{L}_1, \mathcal{L}_2])$$
$$= \text{vec}[\partial_1\sigma]^\dagger \mathcal{R}^{-1}(\bar{\sigma} \otimes \mathbf{K} - \mathbf{K} \otimes \sigma)\mathcal{R}^{-1}\text{vec}[\partial_2\sigma]$$
$$+ 4\partial_1\mathbf{d}^\dagger \sigma^{-1}\mathbf{K}\sigma^{-1}\partial_2\mathbf{d} = 0. \tag{29}$$

From now on, we set $\nu = 1$ for the sake of convenience because this paper is independent of the number of measurements. The QFI matrix can be analytically derived by Eq. (24). However, the general form is verbose. Results are presented by using numerical values, as shown in Figs. 4–6. We define the factor μ as the ratio of the simultaneous uncertainty and the individual uncertainty, i.e.,

$$\mu = \frac{(\delta^2 T_1 + \delta^2 T_2)|_{\text{sim}}}{\delta^2 T_1|_{\text{ind}} + \delta^2 T_2|_{\text{ind}}} = \frac{\mathcal{H}^{11}\mathcal{H}^{22}}{\mathcal{H}^{11}\mathcal{H}^{22} - |\mathcal{H}^{12}|^2}, \tag{30}$$

where the latter equation comes from the saturated QCRB.

From Fig. 4, we can see that in the case of $s = 0.5$, the simultaneous estimation uncertainty is less than the individual uncertainty given by the same resource, i.e., the ratio factor $\mu < 1$. This shows that the simultaneous estimation performs better than the individual estimation. When the temperature
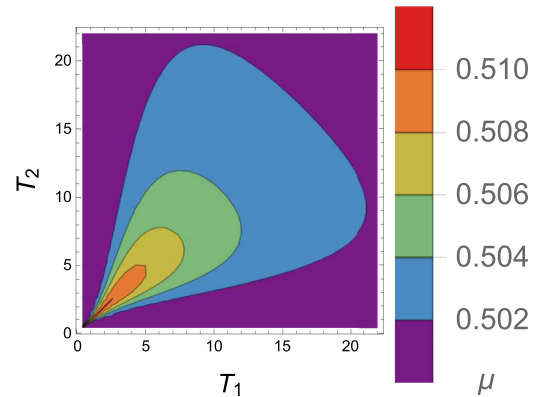

FIG. 3. The ratio $2\mathcal{H}^{11}/\mathcal{F}(T)$, computed from Eq. (27), vs the degree of diffraction s. The dimensionless parameters are given by $\omega = 1$ and $\eta = 0.5$.

FIG. 4. The ratio of the simultaneous uncertainty to the individual uncertainty, μ, vs the two temperatures T_1 and T_2. The dimensionless parameters are given by $\omega = 10$, $\eta = 0.5$, and $s = 0.5$.
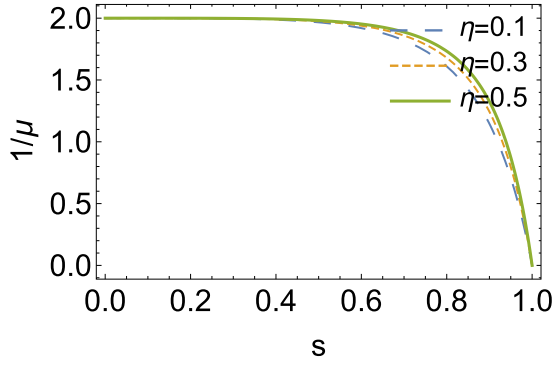
FIG. 5. The ratio between the individual uncertainty and the simultaneous uncertainty, $1/\mu$, vs the degree of diffraction s. The dimensionless parameters are given by $\omega = 10$, $T_1 = 8$, and $T_2 = 10$.

difference ($|T_1 - T_2|$) is relatively large or both temperatures are relatively high ($T_1 \gg \omega$ and $T_2 \gg \omega$), we find that the ratio μ is close to $1/2$. This indicates that simultaneous estimation in this case is a better use of resources to improve measurement precision.

From Fig. 5, we can see that the ratio of the individual uncertainty and the simultaneous uncertainty, $1/\mu$, decreases with the increase in s. In particular, the ratio $1/\mu$ approaches 0 as the diffraction degree approaches 1. This indicates that the advantage of the simultaneous estimation decreases as s increases. At the maximum diffraction, the simultaneous estimation uncertainty will be infinite, which means that the maximum diffraction completely prevents the simultaneous estimation from obtaining the information of both temperatures. In addition, we can see that the attenuation factor η has very little effect on the ratio, especially if s is around 0 and 1.

As shown in Fig. 6, although the individual estimation uncertainty ($\delta^2 T_1|_{\text{ind}} + \delta^2 T_2|_{\text{ind}}$) also increases with s, it is always finite. This means that the individual estimation can obtain the information of the two temperatures when subjected to the maximum diffraction.

V. A PRACTICAL AND FEASIBLE ESTIMATION OF A SINGLE PARAMETER

A simple way to measure the individual estimation error of the single parameter T_i is given by the error transfer
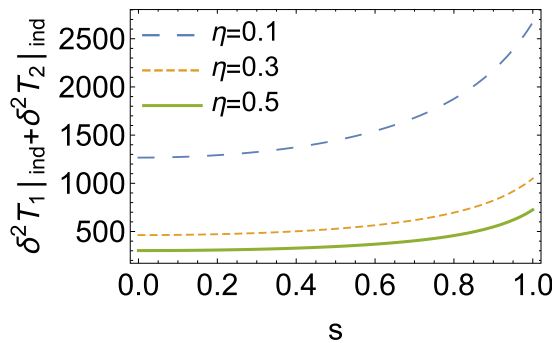

FIG. 6. The individual uncertainty $\delta^2 T_1|_{\text{ind}} + \delta^2 T_2|_{\text{ind}}$ vs the degree of diffraction s. Here, the values of the selected parameters are the same as in Fig. 5.

formula [45,46]

$$(\delta T_i)^2 = (\delta X)^2 / (\partial_i \langle X \rangle)^2, \tag{31}$$

where $(\delta X)^2 = \langle X^2 \rangle - \langle X \rangle^2$ and $\langle \cdot \rangle = \text{tr}[\cdot \rho]$. It just needs to measure the average value of a single measurement observable X.

For a single parameter, Gessner *et al.* [47] provided an analytical optimization over all possible linear combinations of some given possible measurement observables $\mathbf{X} = (X_1, \ldots, X_K)^T$.

With the optimal linear combinations $X_{\mathbf{m}} = \mathbf{m} \cdot \mathbf{X} \propto \Gamma^{-1}[T_i, \mathbf{X}] D[T_i, \mathbf{X}] \cdot \mathbf{X}$, the corresponding optimized measurement sensitivity can be described as

$$M[T_i, \mathbf{X}] = \max_{\tilde{m}} (\partial_i \langle X_{\tilde{m}} \rangle)^2 / (\delta X_{\tilde{m}})^2 \tag{32}$$

$$= \mathbf{D}[T_i, \mathbf{X}]^T \Gamma^{-1}[T_i, \mathbf{X}] \mathbf{D}[T_i, \mathbf{X}], \tag{33}$$

where linear combinations $X_{\tilde{\mathbf{m}}} = \tilde{\mathbf{m}} \cdot \mathbf{X}$, $\mathbf{D}[T_i, \mathbf{X}] = (\partial_i \langle X_1 \rangle, \ldots, \partial_i \langle X_K \rangle)^T$, and the elements of the covariance matrix are $\Gamma_{k,l}[T_i, \mathbf{X}] = \langle X_k X_l \rangle - \langle X_k \rangle \langle X_l \rangle$. The optimized sensitivity given by Eq. (33) is obtained by the measurement coefficient vector $\tilde{\mathbf{m}} = \mathbf{m}$. The measurement sensitivity obeys the chain of inequalities $M[T_i, \mathbf{X}] \leqslant \mathcal{F}[T_i, X_{\mathbf{m}}] \leqslant \mathcal{H}^{ii}$. Here, $\mathcal{F}[T_i, X_{\mathbf{m}}]$ denotes the Fisher information of T_i obtained from the measurement of $X_{\mathbf{m}}$; $\mathcal{H}^{ii}$ denotes the QFI of T_i as shown in Eq. (24).

Photon counting after spatial-mode demultiplexing has been shown to be the measurement that allows one to approach the ultimate limit for the separation estimation [6,26]. Suppose that we have access to K orthonormal spatial modes $\{\upsilon_k(x)\}$ with associated field operators a_k and that the photon number in each mode can be obtained from the photon counting operator $N_k = b_k^\dagger b_k$. $b_k = g_{k+} a_+ + g_{k-} a_-$ with $g_{k\pm} = \int dx \upsilon_k^*(x) \psi_\pm(x)$. Then, the mean photon number in each mode is

$$\langle N_k \rangle = N\eta(|f_{+,k}|^2 + |f_{-,k}|^2) - \gamma N\eta(|f_{+,k}|^2 - |f_{-,k}|^2), \tag{34}$$

where $f_{\pm,k} = \int dx \upsilon_k^*(x) \psi(x \pm d/2)$.

Next, we focus on the case of a Gaussian point-spread function $\psi(x) = \sqrt{2/\pi \varpi^2} \exp(-x^2/\varpi^2)$. For a small average number of photons, demultiplexing Hermite-Gauss (HG) modes can help us to approach the QCRB. Hence we also consider the orthonormal spatial modes

$$\upsilon_k(x) = u_k(x) = \mathcal{N}_k H_n\left(\frac{\sqrt{2}x}{\varpi}\right) e^{-x^2}, \tag{35}$$

where $H_n(x)$ are the Hermite polynomials and the normalization constant $\mathcal{N}_k = [(\pi/2)\varpi^2 2^k k!]^{-1/2}$.

Letting $X_k = N_k$, $\mathbf{X} = \mathbf{N} = (N_1, \ldots, N_K)^T$, the measurement sensitivity of T_i can be obtained by Eq. (33):

$$M[T_i, \mathbf{N}] = (2\eta \partial_i N)^2 \left[\frac{\sum_{k=0}^K \beta_k^2(d)}{2N\eta} - \frac{A_+}{A_+ A_- - B^2} \mathcal{S}_1^2 \right.$$

$$\left. + \frac{2B}{A_+ A_- - B^2} \mathcal{S}_1 \mathcal{S}_2 - \frac{A_-}{A_+ A_- - B^2} \mathcal{S}_2^2 \right], \tag{36}$$

where

$$A_\pm = \frac{2}{1 \pm \gamma^2} + 2N\eta \sum_{k=0}^{K} \beta_k^2(d), \quad (37)$$

$$B = 2N\eta \sum_{k=0}^{K} (-1)^k \beta_k^2(d), \quad (38)$$

$$\mathcal{S}_1 = \sum_{k=0}^{K} (-1)^k \beta_k^2(d), \quad (39)$$

$$\mathcal{S}_2 = \sum_{k=0}^{K} \beta_k^2(d). \quad (40)$$

Here, $\beta_k(d) = f_{\pm,k} = \frac{1}{\sqrt{k!}} \exp[\frac{d^2}{8\varpi^2}](\pm \frac{d}{2\varpi})^k$. When the number of received photons is low $N\eta \ll 1$, the sensitivity can be

simplified as

$$M[T_i, \mathbf{N}] \approx (2\eta \partial_i N)^2 \frac{\sum_{k=0}^{K} \beta_k^2(d)}{2N\eta}$$

$$= \sum_{k=0}^{K} \frac{(\partial_i N_k)^2}{N_k} = N_t \sum_{k=0}^{K} \frac{(\partial_i p_k)^2}{p_k}, \quad (41)$$

where the total number of thermal photons $N_t = \sum_{k=0}^{K} N_k$ and the probability $p_k = N_k/N_t$. The above equation shows that the FI is obtained, which means that the estimation strategy based on the optimized error transfer formula can saturate the Cramér-Rao bound.

When the full HG basis is measured, i.e., $K \longrightarrow \infty$, we can obtain the sensitivity of the single parameter T_i

$$M[T_i, \mathbf{N}] = (2\eta \partial_i N)^2 \left[\frac{1}{2N\eta} - \frac{2s^2(1-\gamma^2) + 2(1+\gamma^2) + 2N\eta(1-\gamma^4)(s-1)^2}{4 + 8N\eta + 4N^2\eta^2(1-s^2)(1-\gamma^4)} \right], \quad (42)$$

where $\partial_i N = \frac{\chi_i \omega}{2T_i^2(1-\chi_i)^2}$. As shown in Fig. 7, the measurement sensitivity $M[T_1, \mathbf{N}]$ gradually approaches the QFI as the degree of diffraction s increases. In other words, as s increases, the estimation strategy based on the optimized error transfer formula tends to be the optimal method by using the full HG basis. At the maximum diffraction $s = 1$, the estimation strategy can saturate the QCRB without being affected by the attenuation factor η.

VI. DIRECT IMAGING

In this section, we calculate the estimation precision of the single parameter T_i obtained by direct imaging. Then, we make a simple comparison with the previous results from the Hermite-Gaussian mode demultiplexing.

The direct imaging estimates the temperature from the density distribution, which is given by

$$I(r) = \langle (\psi_+(x)a_+ + \psi_-(x)a_-)^\dagger (\psi_+(x)a_+ + \psi_-(x)a_-) \rangle$$
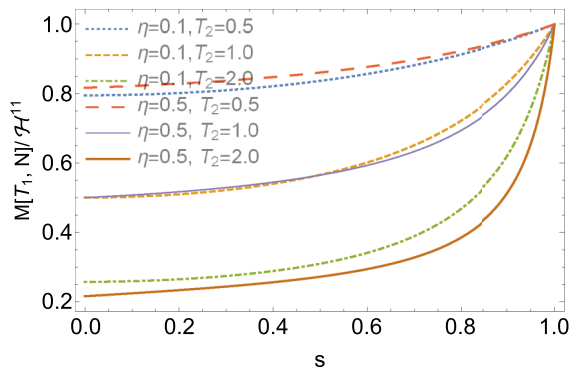$$= N\eta[(1+\gamma)|\psi(x+d/2)|^2 + (1-\gamma)|\psi(x-d/2)|^2]. \quad (43)$$

FIG. 7. The ratio of the measurement sensitivity and the QFI, $M[T_1, \mathbf{N}]/\mathcal{H}^{11}$, vs the degree of diffraction s. Here, the values of the selected dimensionless parameters are given by $\omega = 1$ and $T_1 = 1$.

By dividing by the total photon number $2N$, we can get the probability distribution

$$P(x) = \frac{\eta}{2}[(1+\gamma)|\psi(x+d/2)|^2 + (1-\gamma)|\psi(x-d/2)|^2]. \quad (44)$$

Due to the loss, the probability that no photon is detected is $1 - \eta$. The FI can be achieved:

$$\mathcal{F}(T_i) = \int_\infty^\infty dx (\partial_i P(x))^2/P(x) \quad (45)$$

$$= \int_\infty^\infty dx \eta (\partial_i \gamma)^2 f(x)/2, \quad (46)$$

where the factor $f(x)$ is described by

$$f(x) = \frac{\eta(|\psi(x+d/2)|^2 - |\psi(x-d/2)|^2)^2}{2P(x)}. \quad (47)$$

From the above equations, we can find that the factor $f(x)$ is equal to 0 at the maximum diffraction $s = 1$ ($d = 0$). This leads us to find that the FI of the temperature $\mathcal{F}(T_i)$ is equal to 0. This means that the direct imaging cannot obtain any information of the temperature at the maximum diffraction. In sharp contrast, the HG mode demultiplexing is still able to get the information. At the maximum diffraction, the HG mode demultiplexing is the optimal measurement. This shows that the HG mode demultiplexing can perform better than the direct imaging in terms of temperature estimation in the case of diffraction limitation.

VII. SIMULTANEOUS ESTIMATION WITH A PRACTICAL MEASUREMENT OPERATOR

In this section, we use a practical measurement to estimate the two parameters T_1 and T_2 simultaneously. We consider a simple measurement operator $E = \sum_{k=0}^{\infty} N_k$, which is the direct sum of all the photon counting after the HG spatial-mode demultiplexing. It is independent of the estimation parameters T_i.
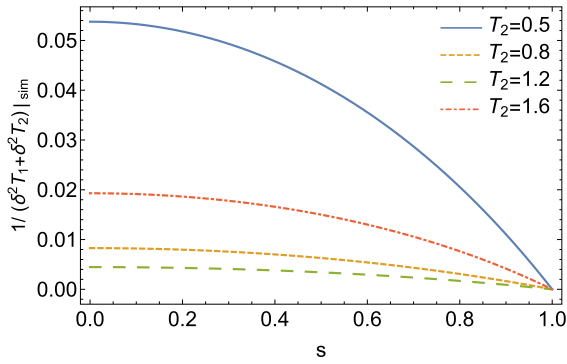
FIG. 8. The reciprocal of the simultaneous estimation uncertainty $\frac{1}{(\delta^2 T_1 + \delta^2 T_2)|_{\text{sim}}}$ obtained by the measurement operator E changes with the degree of diffraction s. Here, the values of the selected dimensionless parameters are given by $T_1 = 1$, $\omega = 1$, and $\eta = 1/2$.

After a simple calculation, we can obtain that $E = \sum_{k=0}^{\infty} N_k = a_+^{\dagger} a_+ + a_-^{\dagger} a_- = (n_+ + n_-)|n_+, n_-\rangle\langle n_+, n_-|$. Conditioned on a detection event, the probability of detecting n_+ and n_- photons in the modes of a_+ and a_- is given by $P_{n_+, n_-} = \langle n_+, n_-|\rho|n_+, n_-\rangle$, which can be further expressed as

P_{n_+, n_-}

$$= \frac{(1 - \gamma^2)^{1 + n_+ + n_-} N_+^{n_+} N_-^{n_-} \, _2F_1\left[1 + n_+, 1 + n_-, 1, \frac{\gamma^2}{\lambda_+ \lambda_-}\right]}{\lambda_+^{n_+ + 1} \lambda_-^{n_- + 1}},$$

(48)

where the parameters in the denominator are $\lambda_{\pm} = 1 + N_{\pm} - N_{\pm}\gamma^2$ and the hypergeometric function $_2F_1[1 + n_+, 1 + n_-, 1, \frac{\gamma^2}{\lambda_+ \lambda_-}] = \sum_{m=0}^{\infty} \frac{[(1+n_+)(1+n_-)\frac{\gamma^2}{\lambda_+ \lambda_-}]^m}{m!}$.

With this measurement probability, the FI can be calculated by

$$\mathcal{F}_C^{ij} = \sum_{n_+, n_- = 0}^{\infty} \frac{\partial_i P_{n_+, n_-} \partial_j P_{n_+, n_-}}{P_{n_+, n_-}}.$$

(49)

As shown in Fig. 8, the reciprocal of the simultaneous estimation uncertainty $\frac{1}{(\delta^2 T_1 + \delta^2 T_2)|_{\text{sim}}}$ decreases with the degree of diffraction s. When $s = 1$, $\frac{1}{(\delta^2 T_1 + \delta^2 T_2)|_{\text{sim}}} = 0$. This shows that the diffraction will reduce the precision of the simultaneous estimation with the practical measurement operator E, which cannot obtain any information at the maximum diffraction. These results support the previous results using the saturated QCRB as shown in Sec. IV B.

VIII. CONCLUSION

We have investigated the effect of diffraction on quantum thermometry. When we know *a priori* that the temperatures of the two thermal sources are always equal, the diffraction will reduce the estimation precision, but not by much: At low temperature, the diffraction has little effect on the estimation precision; at high temperature, the maximum diffraction yields half as much QFI as no diffraction. More QFI can be obtained with the *a priori* information (the two temperatures are always equal) than without the *a priori* information (i.e.,

the two temperatures of the two thermal sources are independent). In particular, at the maximum diffraction, the *a priori* information can help us to obtain twice as much QFI as can be obtained without the *a priori* information. What is more, we carefully consider two strategies: simultaneous estimation and individual estimation. The simultaneous estimation of two temperatures is proved to satisfy the saturation condition of QCRB. Given the same resources, the simultaneous estimation performs better than the individual estimation in the case of a small degree of diffraction. However, in the case of a high degree of diffraction, the individual estimation performs better. In particular, at the maximum diffraction, the simultaneous estimation cannot get any information, which is supported by a practical measurement, while the individual estimation can still get the information. In addition, we find that for the individual estimation, a practical and feasible estimation strategy based on the optimized error transfer formula can saturate the Cramér-Rao bound when the number of received photons is low. At the maximum diffraction, the practical and feasible estimation strategy using the full HG basis can saturate the QCRB without being affected by the attenuation factor. The HG mode demultiplexing can achieve higher temperature estimation precision than the direct imaging in the case of diffraction limitation.

Since the focus of our research is temperature estimation, we assume that the separation of the two thermal sources is known. It is difficult to precisely estimate the separation using conventional technology when the intensity distribution of the two sources on the image plane is close. Spatial-mode demultiplexing has been shown to greatly enhance the precision of the separation estimation [48]. More importantly, experimentally, the positions of the two light sources can be controlled in advance, rather than measured on the imaging plane. In addition, multiple parameters including separation and temperature can also be measured simultaneously using the QFI matrix. The impact of the unknown centroid and separation of the two thermal sources on the estimation of temperatures deserves further study. Our study illustrates the effect of diffraction on the temperature measurement precision and the advantages and disadvantages of different measurement strategies, which lays a foundation for constructing a remote precision thermometry to obtain surface temperature distributions [49,50].

APPENDIX: THE DENSITY MATRIX ON THE IMAGE PLANE

We now use Eq. (9) to propagate the density matrix ρ_0 of the sources to the density matrix ρ on the image plane.

When we transform the coherent state $|\alpha_1, \alpha_2\rangle$ of the field operators c_1 and c_2 to the coherent state $|\alpha_+, \alpha_-\rangle$ of the field operators $a_\pm$, we can obtain the following mapping relation according to Eq. (9) and the auxiliary modes in the vacuum state

$$\sqrt{\eta_+}c_\pm|\alpha_1, \alpha_2\rangle\langle\alpha_1, \alpha_2| \rightarrow a_\pm|\alpha_+, \alpha_-\rangle\langle\alpha_+, \alpha_-|$$

$$\Rightarrow \sqrt{\eta_\pm/2}(\alpha_1 \pm \alpha_2)|\alpha_1, \alpha_2\rangle\langle\alpha_1, \alpha_2| \rightarrow \alpha_\pm|\alpha_+, \alpha_-\rangle\langle\alpha_+, \alpha_-|.$$

$$\text{(A1)}$$

Based on above equations, we obtain the mapping relations

$$\alpha_1 \rightarrow \alpha_{1+} = \alpha_+/\sqrt{2\eta_+} + \alpha_-/\sqrt{2\eta_-}; \qquad \text{(A2)}$$

$$\alpha_2 \rightarrow \alpha_{2-} = \alpha_+/\sqrt{2\eta_+} - \alpha_-/\sqrt{2\eta_-}. \qquad \text{(A3)}$$

Then, with the two equations above we further obtain

$$\int d^2\alpha_1 d^2\alpha_2 P_{c_1,c_2}(\alpha_1, \alpha_2)|\alpha_1, \alpha_2\rangle\langle\alpha_1, \alpha_2|$$

$$\rightarrow \int d^2\alpha_{1+} d^2\alpha_{2-} P_{c_1,c_2}(\alpha_{1\pm}, \alpha_{2\pm})|\alpha_+, \alpha_-\rangle\langle\alpha_+, \alpha_-|$$

$$\text{(A4)}$$

$$= \int d^2\alpha_+ d^2\alpha_- P_{a_+,a_-}(\alpha_+, \alpha_-)|\alpha_+, \alpha_-\rangle\langle\alpha_+, \alpha_-|. \quad \text{(A5)}$$

At this point, Eq. (10) has been derived.

---

[1] L. Rayleigh, XXXI. Investigations in optics, with special reference to the spectroscope, London, Edinburgh, Dublin Philos. Mag. J. Sci. **8**, 261 (1879).

[2] M. Born and E. Wolf, *Principles of Optics: Electromagnetic Theory of Propagation, Interference and Diffraction of Light* (Elsevier, New York, 2013).

[3] S. W. Hell and J. Wichmann, Breaking the diffraction resolution limit by stimulated emission: Stimulated emission-depletion fluorescence microscopy, Opt. Lett. **19**, 780 (1994).

[4] T. A. Klar, S. Jakobs, M. Dyba, A. Egner, and S. W. Hell, Fluorescence microscopy with diffraction resolution barrier broken by stimulated emission, Proc. Natl. Acad. Sci. USA **97**, 8206 (2000).

[5] E. Betzig, G. H. Patterson, R. Sougrat, O. W. Lindwasser, S. Olenych, J. S. Bonifacino, M. W. Davidson, J. Lippincott-Schwartz, and H. F. Hess, Imaging intracellular fluorescent proteins at nanometer resolution, Science **313**, 1642 (2006).

[6] M. Tsang, R. Nair, and X.-M. Lu, Quantum Theory of Super-resolution for Two Incoherent Optical Point Sources, Phys. Rev. X **6**, 031033 (2016).

[7] S. Z. Ang, R. Nair, and M. Tsang, Quantum limit for two-dimensional resolution of two incoherent optical point sources, Phys. Rev. A **95**, 063847 (2017).

[8] Z. Yu and S. Prasad, Quantum Limited Superresolution of an Incoherent Source Pair in Three Dimensions, Phys. Rev. Lett. **121**, 180504 (2018).

[9] C. Napoli, S. Piano, R. Leach, G. Adesso, and T. Tufarelli, Towards Superresolution Surface Metrology: Quantum Estimation of Angular and Axial Separations, Phys. Rev. Lett. **122**, 140505 (2019).

[10] B. Wang, L. Xu, J. Li, and L. Zhang, Quantum-limited localization and resolution in three dimensions, Photonics Res. **9**, 1522 (2021).

[11] L. J. Fiderer, T. Tufarelli, S. Piano, and G. Adesso, General expressions for the quantum Fisher information matrix with applications to discrete quantum imaging, PRX Quantum **2**, 020308 (2021).

[12] M. Tsang, Subdiffraction incoherent optical imaging via spatial-mode demultiplexing, New J. Phys. **19**, 023054 (2017).

[13] S. Zhou and L. Jiang, Modern description of Rayleigh's criterion, Phys. Rev. A **99**, 013808 (2019).

[14] M. Tsang, Quantum limit to subdiffraction incoherent optical imaging, Phys. Rev. A **99**, 012305 (2019).

[15] C. Lupo, Z. Huang, and P. Kok, Quantum Limits to Incoherent Imaging are Achieved by Linear Interferometry, Phys. Rev. Lett. **124**, 080503 (2020).

[16] L. Peng and X. Lu, Generalization of Rayleigh's criterion on parameter estimation with incoherent sources, Phys. Rev. A **103**, 042601 (2021).

[17] C. Lupo, Subwavelength quantum imaging with noisy detectors, Phys. Rev. A **101**, 022323 (2020).

[18] C. Oh, S. Zhou, Y. Wong, and L. Jiang, Quantum Limits of Superresolution in a Noisy Environment, Phys. Rev. Lett. **126**, 120502 (2021).

[19] G. Sorelli, M. Gessner, M. Walschaers, and N. Treps, Optimal Observables and Estimators for Practical Superresolution Imaging, Phys. Rev. Lett. **127**, 123604 (2021).

[20] T. M. Stace, Quantum limits of thermometry, Phys. Rev. A **82**, 011611 (2010).

[21] A. De Pasquale and T. M. Stace, Quantum thermometry, in *Thermodynamics in the Quantum Regime: Fundamental Aspects and New Directions*, edited by F. Binder, L. A. Correa, C. Gogolin, J. Anders, and G. Adesso (Springer, Cham, 2018), pp. 503–527.

[22] M. Mehboudi, A. Sanpera, and L. A Correa, Thermometry in the quantum regime: recent theoretical progress, J. Phys. A: Math. Theor. **52**, 303001 (2019).

[23] M. Fujiwara and Y. Shikano, Diamond quantum thermometry: From foundations to applications, Nanotechnology **32**, 482002 (2021).

[24] P. R. N. Childs, J. R. Greenwood, and C. A. Long, Review of temperature measurement, Rev. Sci. Instrum. **71**, 2959 (2000).

[25] D. L. Blackburn, *Temperature measurements of semiconductor devices - a review, in Twentieth Annual IEEE Semiconductor Thermal Measurement and Management Symposium* (IEEE, Piscataway, NJ, 2004), pp. 70–80.

[26] R. Nair and M. Tsang, Far-Field Superresolution of Thermal Electromagnetic Sources at the Quantum Limit, Phys. Rev. Lett. **117**, 190801 (2016).

[27] G. Sorelli, M. Gessner, M. Walschaers, and N. Treps, Moment-based superresolution: Formalism and applications, Phys. Rev. A **104**, 033515 (2021).

[28] C. W. Helstrom, *Quantum Detection and Estimation Theory* (Academic, New York, 1976).

[29] M. G. Genoni, M. G. A. Paris, G. Adesso, H. Nha, P. L. Knight, and M. S. Kim, Optimal estimation of joint parameters in phase space, Phys. Rev. A **87**, 012107 (2013).

[30] P. C. Humphreys, M. Barbieri, A. Datta, and I. A. Walmsley, Quantum Enhanced Multiple Phase Estimation, Phys. Rev. Lett. **111**, 070403 (2013).

[31] M. A. Ciampini, N. Spagnolo, C. Vitelli, L. Pezze, A. Smerzi, and F. Sciarrino, Quantum-enhanced multiparameter estimation in multiarm interferometers, Sci. Rep. **6**, 28881 (2016).

[32] J. Liu, X.-M. Lu, Z. Sun, and X. Wang, Quantum multiparameter metrology with generalized entangled coherent state, J. Phys. A: Math. Theor. **49**, 115302 (2016).

[33] P. Kok, J. Dunningham, and J. F. Ralph, Role of entanglement in calibrating optical quantum gyroscopes, Phys. Rev. A **95**, 012326 (2017).

[34] D. Xie and C. Xu, Quantum estimation of detection efficiency with no-knowledge quantum feedback, Chin. Phys. B **27**, 060303 (2018).

[35] D. Branford, H. Miao, and A. Datta, Fundamental Quantum Limits of Multicarrier Optomechanical Sensors, Phys. Rev. Lett. **121**, 110505 (2018).

[36] W. Ge, K. Jacobs, Z. Eldredge, A. V. Gorshkov, and M. Foss-Feig, Distributed Quantum Metrology with Linear Networks and Separable Inputs, Phys. Rev. Lett. **121**, 043604 (2018).

[37] Q. Zhuang, Z. Zhang, and J. H. Shapiro, Distributed quantum sensing using continuous-variable multipartite entanglement, Phys. Rev. A **97**, 032329 (2018).

[38] D. Xie and C. Xu, Multi-parameter quantum magnetometry with spin states in coarsened measurement reference, Quantum Inf. Proc. **18**, 241 (2019).

[39] J. Yang, S. Pang, Y. Zhou, and A. N. Jordan, Optimal measurements for quantum multiparameter estimation with general states, Phys. Rev. A **100**, 032104 (2019).

[40] X.-M. Lu and X. Wang, Incorporating Heisenberg's Uncertainty Principle into Quantum Multiparameter Estimation, Phys. Rev. Lett. **126**, 120503 (2021).

[41] H. Chen, Y. Chen, and H. Yuan, Information Geometry Under Hierarchical Quantum Measurement, Phys. Rev. Lett. **128**, 250502 (2022).

[42] H. Chen, Y. Chen, and H. Yuan, Incompatibility measures in multiparameter quantum estimation under hierarchical quantum measurements, Phys. Rev. A **105**, 062442 (2022).

[43] S. Ragy, M. Jarzyna, and R. Demkowicz-Dobrzanski, Compatibility in multiparameter quantum metrology, Phys. Rev. A **94**, 052108 (2016).

[44] D. Šafránek, Estimation of Gaussian quantum states, J. Phys. A: Math. Theor. **52**, 035304 (2019).

[45] G. Tóth and I. Apellaniz, Quantum metrology from a quantum information science perspective, J. Phys. A: Math. Theor. **47**, 424006 (2014).

[46] S. L. Braunstein and C. M. Caves, Statistical Distance and the Geometry of Quantum States, Phys. Rev. Lett. **72**, 3439 (1994).

[47] M. Gessner, A. Smerzi, and L. Pezz, Metrological Nonlinear Squeezing Parameter, Phys. Rev. Lett. **122**, 090503 (2019).

[48] P. Boucher, C. Fabre, G. Labroille, and N. Treps, Spatial optical mode demultiplexing as a practical tool for optimal transverse distance estimation, Optica **7**, 1621 (2020).

[49] J. Oh, G. Lee, J. Rho, S. Shin, B. Lee, Y. Nam, and Y. Park, Optical Measurements of Three-Dimensional Microscopic Temperature Distributions Around Gold Nanorods Excited by Localized Surface Plasmon Resonance, Phys. Rev. Appl. **11**, 044079 (2019).

[50] T. Emig, Temperature distribution and heat radiation of patterned surfaces at short wave lengths, Phys. Rev. E **95**, 052104 (2017).